Combination of Na-Ca-phosphate and fluorapatite in wollastonite-diopside glass-ceramic: degradation and biocompatibility

Ebrahim A. Mahdy
National Research Centre
Hanaa Y. Ahmed
Al-Azhar University
Mohammad Farag (mmfaragnrc@gmail.com)
National Research Centre https://orcid.org/0000-0001-5069-9030

Research Article

Keywords: Wollastonite, Diopside, Sodium calcium phosphate, Fluorapatite, Glass-ceramic, Bioactivity

Posted Date: March 3rd, 2021

DOI: https://doi.org/10.21203/rs.3.rs-284151/v1

Abstract

In this study, we investigated the effect of introducing sodium calcium phosphate (NCP), fluorapatite (FA), or the combination of both phases in the wollastonite-diopside (WD) bioactive glass-ceramic system on the crystalline phases formed, microstructure, degradation, and biocompatibility of those materials. The prepared materials were characterized by DTA, XRD, and SEM/EDX. Moreover, the density was measured via Archimede's method, and the mechanical properties were measured by Vicker's microhardness indenter. The in vitro bioactivity test was carried out in the simulated body fluid (SBF), and the cell viability test was evaluated using the Vero cells. The results showed that the formed crystalline phases were close to the starting proposed phases. Moreover, NCP-containing WD glass-ceramic was showed the lowest density value due to its low densification, and accordingly, it showed the lowest Vicker`s microhardness value due to the same reason. Furthermore, combining sodium calcium phosphate in WD glass-ceramic was increased cell viability better than that included fluorapatite, whereas, the combination of both crystalline phases in WD glass-ceramic led to an increase in the cytotoxicity to the highest value. In conclusion, different properties of wollastonite-diopside glass-ceramics can be tailored by the combination of NCP or FA, and hence, these glass-ceramic materials can be modified effectively according to the purpose for which it is intended to be applied. The obtained results indicated that different properties of WD glass-ceramic materials can be tailored by the combination of NCP and/or FA. Hence, these glass-ceramics are expected to be useful materials in promising biomedical applications, such as orthopedics and dentistry.

1. Introduction

Glass-ceramic materials have to pay more attention to the biomedical uses meanwhile the innovation of bioglass in 1971 by Hench, et al [1]. They are being used broadly for biomedical requests as orthopedic implant and bone filler materials, as a result of their biocompatibility and tight bonding with bone [2, 3]. The bioactive glass-ceramics have a significant place in the biomedical application, due to their higher mechanical strength compared to the derived glass thanks to their unique microstructure [4–6]. Moreover, they are capable to bond with the living bone directly by the growth of healthy tissue onto their surface through a biologically active hydroxycarbonate apatite (HCA) layer without the formation of surrounding fibrous tissue. The HCA phase that forms on the bioactive glass-ceramic surfaces is chemically and structurally equivalent to the mineral phase of the bone. This correspondence has an effective role in the interfacial connecting between the bioactive material and bone [7].

Among various silicate materials, pyroxene glass-ceramics had created a global interest for several applications recently [8–11] in material science and technology owing to a brilliant set of physical properties. Diopside ($CaMgSi_2O_6$) is a significant member of the pyroxenes class. Glass-ceramic materials based on diopside have high mechanical and excellent chemical properties with more distinct biological activity. These properties make them interested in biomedical applications as bone tissue engineering [10, 12–16]. Glass-ceramics containing wollastonite ($CaSiO_3$) crystals are promising candidates

for bone tissue regeneration as a result of their great mechanical properties, good bioactivity, and biocompatibility [17, 18]. The presence of wollastonite crystals in glass-ceramics was reported to increase the strength and toughness of those materials [19]. Expectedly, combining diopside and wollastonite crystals is likely to produce glass-ceramics with excessive mechanical strength and outstanding bioactive properties. Accordingly, there have been several works that studied diopside-wollastonite glass-ceramics for biomedical applications. Therefore, wollastonite-diopside glass-ceramics have been used widely for orthopedics and bone regeneration applications [20–24]. Moreover, this glass-ceramic system was modified by the addition of other crystalline phases, such as tricalcium phosphate, fluorapatite, and sodium calcium phosphate.

Fluorapatite glass-ceramics are superior materials for bone grafting and dental applications thanks to the antibacterial properties of the fluorine ion [25]. Kokubo, et al. were the first authors' combined apatite with wollastonite to prepare the binary apatite-wollastonite glass-ceramics with better mechanical properties [26]. The phase formation in the fluorapatite–diopside binary system was studied as a new type of bioglass–ceramics possessed high chemical and mechanical properties with great biocompatibility [27]. Furthermore, fluorapatite has been introduced to wollastonite-diopside glass-ceramic to impart more potential properties for different biomedical applications [28, 29]. For developing biomaterials with talent properties, Salinas, et al. [2] were succeeded to prepare bioactive glass-ceramics depending on the ternary $Ca_3(PO4)_2–CaSiO_3–CaMgSi_2O_6$ system. Salman, et al. [30] prepared glass-ceramic based on $CaMgSi_2O_6–CaSiO_3–Ca_5(PO_4)_3F–Na_2SiO_3$ system with TiO_2 or ZnO additives. They stated that, by in vitro results, the glass-ceramics containing Na-Ca silicate showed higher bioactivity to be suitable for restorative dental and bone-implant materials. Herein, we aimed to study the effect of introducing of $Na_4Ca(PO_3)_6$ and/or $Ca_5(PO_4)_3F$ phases in the wollastonite-diopside bioactive glass-ceramic system on the physicochemical properties, such as density, degradation, and biocompatibility, as well as, the mechanical properties (microhardness) of the resulting glass-ceramics for biomedical uses as bone replacement materials. The crystalline phases formed and microstructure characterization are also studied.

2. Materials And Methods

2.1. Glass synthesis

The batch compositions were designed depending on the weight proportions of diopside–wollastonite–sodium calcium phosphate–fluoroapatite phases as presented in Table 1. The glass samples were prepared via a conventional melt-quenching technique. The calculated weights of high purity (> 99.9 %) grade reagent powders calcium carbonate ($CaCO_3$), magnesium carbonate ($MgCO_3$), sodium carbonate (Na_2CO_3), ammonium di-hydrogen phosphate ($NH_4H_2PO_4$), calcium fluoride (CaF_2), and silica (SiO_2) were well thoroughly mixed. The mixed powders were melted in alumina crucible at 1400–1450°C for 3 h in an electric furnace (Carbolite HTC 1600, Vechstar). The melting process was continued with stirring until

clear homogeneity. Then, the melts were cast on a preheated stainless steel mold in the designed shapes. The cast glass species were moved to an annealing furnace at 450°C in an electric furnace. Then, the furnace turns off after 1 h and allowed to cool naturally to room temperature for preparing hard glass samples free from strain and stress.

2.2. Differential Thermal Analysis (DTA)

All prepared glass samples were analyzed by Differential Thermal Analysis (DTA-SDTQ600–TA Instruments, USA) to determine their critical thermal characteristics such as the glass transition temperatures (Tg), crystallization temperatures (Tc), and any other endotherms up to 1100°C. A very finer 30 mg powder of each glass sample (< 38 μm) were analyzed in alumina crucible using analytical grade alumina powder as a reference with a heating rate of 10°C/min from room temperature up to 1100°C in a flowing nitrogen atmosphere.

Table 1
Theoretical phase components with corresponding oxide constituents.

Sample ID.	Theoretical phase components (wt.%)				Oxide constitutions (wt.%)					
	Dio	Wo	NCP	FA	CaO	MgO	Na_2O	SiO_2	P_2O_5	CaF_2
WD1	80	20	-	-	30.37	14.88	-	54.75	-	-
WD 2	70	20	10	-	28.71	13.02	2.05	49.20	7.02	-
WD3	70	20	-	10	32.78	13.02	-	49.20	4.22	0.78
WD4	60	20	10	10	31.12	11.16	2.05	43.65	11.24	0.78

*__Dio__ = Diopside-$CaMgSi_2O_6$, __Wo__ = Wollastonite-$CaSiO_3$, __NCP__ = Sodium calcium phosphate-$Na_4Ca(PO_3)_6$, __FA__ = Fluoroapatite-$Ca_5(PO_4)_3F$

2.3. Glass-ceramic preparation

Double stage heat-treatment schedules were applied to investigate the glass-ceramic materials via the controlled crystallization process of glasses. According to the DTA data, each glass composition was heat-treated for 3 h near the glass transition temperature, in the first stage, to provide adequate nucleation sites which occur nearly in the endothermic temperature. Then, the temperature was raised to the exothermic temperature for 6 h, in which the crystal growth was expected (the second stage) at a constant heating rate of 10°C/min.

2.4. X-ray diffraction analysis (XRD)

The developed crystalline phases of the glass-ceramic specimens were identified employing the X-ray powder diffractometer (XRD, PANalytical PW3040/60, Netherlands). Cu-Kα radiation source (λ = 1.5401 Å), was used with generated at 30 mA and 45 kV with a scan speed of 2°/min over a 2θ-range of 5–75°.

The diffraction Peaks of the investigated crystalline phase are analyzed with JCPDS files and noticeable with different symbols.

2.5. Microstructure study (SEM)

The microstructure of the investigated glass-ceramic samples was analyzed for studying the internal morphology of the crystal phases formed. The fractured surfaces for the selected samples were immersed in a 2 vol% HF as an etching solution for one minute to remove the residual glassy phase. Then the samples were washed with distilled water and their fractured surfaces were coated with a thin film of Au, by SEM Coating unit, to reduce any charging effects. Finally, they were observed by using scanning electron microscopy (SEM/EDS, Quanta FEG 250, Netherlands) that operated at an acceleration voltage of 20 kV.

2.6 The density test

The apparent density of the bulk glass-ceramic samples was measured, to an accuracy of (± 0.0002) via the Archimedes method by immersion all specimens in distilled water as buoyant liquid. The mean and the standard deviation values are shown for density have been achieved from at least 6 different specimens for each sample. Molar volume was calculated using the obtained density data for all measured samples of the bulk glass-ceramics.

2.7. The Mechanical properties (Vicker's microhardness)

The microhardness of the investigated glass-ceramics was measured to study the mechanical properties using a Vicker's microhardness indenter (ModelHV-100 microhardness tester) with an applied load of 100 g fixed for all samples for 15 s. For indentation testing, all glass-ceramic specimens were cut and polished carefully to find flat and smooth parallel surfaces for each specimen. At least 7 Vickers impressions were made on the polished surface of each sample with an estimated accuracy of (± 0.5 μm). The final hardness value was calculated from Eq. (1):

$$Hv\ (kg/mm2\ ) = A\ (P/d2)\ (1)$$

A is a constant equal to 1854.5, P is the applied load (g) and d is the average diagonal length (mm). The microhardness values are changed from kg/mm2 to MPa by multiplying with a constant value of 9.8.

2.8. In vitro bioactivity test

The glass-ceramic degradation was carried out in the simulated body fluid (SBF), prepared as described previously [31]. The bulk glass samples of 0.2 g were immersed in 15 ml SBF for 1, 3, and 7, 14, and 22 d at 37°C. At the predetermined period, the pH of the soaking solution was measured by pH meter (3040 Ion Analyzer), and the sample was removed from the solution and dried at 70°C, and then weighed by the electronic balance of four decimals. The weight loss (%) was calculated under Eq. (2).

$$\text{Wt. loss } \% = (W_i - W_d/W_i) \times 100\ (2)$$

Where, Wi and Wd are the initial weight and weight after soaking in SBF, respectively. The whole immersing solution was collected and replaced by a fresh one, and the concentrations of ions released ($Ca^{2+}$and PO_4^{3-}, K^+) from the glass-ceramic samples were measured using colorimetric kits (BIODIGNOSTIC, Egypt). Furthermore, the change of glass-ceramic surfaces after immersion in SBF was assessing by SEM/EDX (Model Quanta 250 FEG (Field Emission Gun) attached with EDX Unit (Energy Dispersive X-ray Analyses), with accelerating voltage 30 KV).

2.9. Cell viability test

2.9.1. MTT assay

The cytotoxic effect was determined against the Vero cell line for WD1, WD2, WD3, and WD4. The cytotoxic test was conducted when the Vero cells reached confluence (75–90%) (usually 1 d). At this time, a suspension of the cell was prepared in the growth medium (DMEM) accompanied with 50 $mg.ml^{-1}$ of gentamycin. 100 µl of cell suspension (number of cells ~ 1 × 105) was added to each well on a 96-well tissue culture plate, and the complete DMEM medium without cells was used as a blank sample. The cells were incubated for 24 h at 37°C in a humidified incubator with 5% CO_2. After the formation of a complete monolayer cell sheet in each well of the plate, the glass samples were added. Different concentrations of (500, 250, 125, 62.5, 31.25, and 15.63 $mg.ml^{-1}$) of glass-ceramic samples were added into a 96-well tissue culture plate containing the cells and incubated for 37°C for 24 h. And then, 100 mL of MTT was cultured with the cell culture supernatant at 37°C with 100 mL of MTT solution (5 $mg.ml^{-1}$) for 4 h, thereafter, the absorbance was detected of such solution was measured at 570 nm using a microplate ELISA reader (SunRise TECAN, USA). The absorbance of untreated cells was considered as 100 % [32].

2.9.2. Microscopic Studies

After the end of the treatment, the wells were washed three times with 100 µl of phosphate-buffered saline (pH 7.2), and then the cells were fixed to the plate with 10 % formalin for 15 min. The fixed cells were then stained with crystal violet solution. After drying, the cellular morphology was investigated using an inverted microscope (CKX41; Olympus, Japan).

3. Results And Discussion

3.1. DTAanalysis

The thermal behavior of the studied glasses was explored by the DTA technique to identify the glass transition (Tg) and glass crystallization temperatures (Tc) which are useful to determine the most appropriate crystallization temperatures for each composition. Figure 1 and Table 2 represent the characteristic transition temperatures (Tg) and crystallization temperatures (Tc), for the obtained glasses as detected from DTA traces. The DTA analysis of the base composition (sample WD1) showed that an endothermic peak effect appeared at 747 oC. This effect indicative for the Tg, at which the atoms begin

to arrange themselves in preliminary structure elements formerly the crystallization step. On the other hand, an exothermic peak was detected at 1038 oC represented the Tc, at which the growth of crystals has occurred completely. The recorded data revealed that additions of 10 wt.% of sodium calcium phosphate-$Na_4Ca(PO_3)_6$ (sample WD2) or flourapatite-$Ca_5(PO_4)_3F$ (sample WD3) at the expense of diopside$CaMgSi_2O_6$ phase in WD1 composition led to a decrease in the Tg to lower temperature from 747 ^oC to 733 ^oC (Fig. 1). Introducing of both $Na_4Ca(PO_3)_6$ and $Ca_5(PO_4)_3F$ phases instead of 20 wt.% $CaMgSi_2O_6$ phase (sample WD4) in the base glass composition led to a reduction of both Tg and Tc to lower temperatures (721°C and 1027°C, respectively). This can be attributed to the effect of Na_2O to decline the glass viscosity and accelerating the nucleation stage. Denry and Holloway [32] reported that the sodium acts as a glass network modifier capable of lowering the viscosity of silicate glasses by increasing the number of non-bridging oxygen in the glass composition. As a result of the decrease in the viscosity, the mobility and diffusion rates of the different ions and ionic complexes forming glasses during the crystallization process will be markedly increased, leading to higher crystallization tendency. Introducing of Na_2O in the glass composition enhanced its crystallization tendency, leading to displacing of Tg and Tc towards lower temperatures. Similarly, P_2O_5 additions to the silicate glass composition led to accelerating volume nucleation and support glass-ceramic formation [33].

3.2. XRD analysis

The existence of various phases formed in the studied glasses was a function of the synthesized glass compositions and the crystallization parameters used. The XRD patterns of the investigated glass-ceramics (WD1, WD2, WD3, and WD4) are displayed in Fig. 2 and the crystalline phases developed by the reheating glasses are given in Table 2. It can be noticed from the figure that the diffraction pattern of the base glass sample (Fig. 2, pattern I), WD1 heat-treated at 745 ^oC/3h-1040 ^oC/6h, was crystallized into pyroxene members of diopsidic-type ($CaMgSi_2O_6$) as a major phase (PDF # 17–0318) beside wollastonite-$CaSiO_3$ phase (PDF # 27-1064). Diopside and wollastonite phases are proper varieties of pyroxene minerals in which the developed glass-ceramics have high mechanical strength and great chemical durability [34]. Glass-ceramics with high Ca contents possess a high ability of good apatite mineralization with excellent bioactive properties [35].

The addition of 10 wt.% sodium calcium phosphate at the expense of 10 wt.% diopside phase in the base composition, i.e. WD2, heat-treated at 730 ^oC/3h-1065 ^oC/6h, led to the crystallization of sodium calcium phosphate phase with a new formula -$Na_4Ca(PO_3)_3$ (PDF # 23–0669) in addition to diopside (as a major phase) and wollastonite phases as proved by the X-ray diffraction analysis (Fig. 2, Pattern II). Whereas, introducing of 10 wt.% fluoroapatite phase at the expense of the diopside phase (glass sample WD3 heated at 735 ^oC/3h-1075 ^oC/6h) resulted in the development of fluoroapatite (PDF # 74-4390) as a new phase together with the major diopside phase. The existence of the wollastonite phase as a secondary phase was also detected as indicated from XRD patterns (Fig. 2, pattern III). More Ca^{2+} ions are included in the media with P^{5+} ions which have a higher ionic field strength, and hence a greater tendency to

shielding. It was also reported that P_2O_5 had a high tendency to react with CaO [36]. Thus, fluoroapatite-$Ca_5(PO_4)_3F$ crystallized from the droplet phase with highly concentrated Ca and P in the presence of CaF_2 in the media [37]. On further decreasing the diopside components by replacing 20 wt.% of $CaMgSi_2O_6$ phase with 10 wt.% of $Na_4Ca(PO_3)_6$ and 10 wt.% of $Ca_5(PO_4)_3F$ in the base composition (glass sample WD4 heat-treated at 720 ^oC/3h-1025 ^oC/6h) resulted in a formation of various crystalline phases, which were diopside, wollastonite, fluoroapatite and sodium calcium phosphate phases as detected by the X-ray diffraction analysis (Fig. 2, pattern IV). The high content of CaO and P_2O_5, by introducing both $Na_4Ca(PO_3)_6$, $Ca_5(PO_4)_3F$ phases, leads to intense phase separation in the glass. Therefore, phase separation is likely to occur, and the phosphate-rich and silicate-rich phases are separated from the parent glass [37].

3.3. SEM analysis

The SEM images for the WD1, WD2, WD3, and WD4 glass-ceramic samples are displayed in Fig. 3 which presents different morphological shapes as a function of oxide content and crystalline phases formed. It was clear from the figure that the volume crystallization of tiny aggregates–like growths was the distinctive microstructure formed in the WD1 sample (Fig. 3a). The introducing of 10 wt.% $Na_4Ca(PO_3)_6$ was caused a change in the crystals microstructure to become dendritic like-growths with some glassy matrix in-between as seen in the micrograph of the WD2 sample (Fig. 3b). Whereas, the volume crystallization of globular grains were the distinctive shape in the WD3 sample with 10 wt.% of $Ca_5(PO_4)_3F$ (Fig. 3c). The replacement of diopside by both $Na_4Ca(PO_3)_6$ (10 wt.%) and $Ca_5(PO4)_3F$ phases (10 wt.%) in the base composition (sample WD4) led to developing bundles of oriented long rods with aggregates of spherical crystals (Fig. 3d).

3.4. Density

The obtained average values of the measuring density in the laboratory by Archimedes method for the bulk glass-ceramic species heat-treated at different temperatures are presented in Table 2 and Fig. 4a. The general trend of increasing the density for bulk glass-ceramic than that in the corresponding glass was caused by an increase in the temperature during the heat treatment process, which led to the elimination of the remaining pores or due to the growth of more amounts of denser crystalline phases [11]. The density of WD1 glass-ceramic was 2.76 g/cm^3, whereas, it was 2.50 g/cm^3, 2.92 g/cm^3, and 2.90 g/cm^3 for WD2, WD3, and WD4 glass-ceramic samples, respectively. The obtained density data revealed that the WD2 glass-ceramic was had the lowest value of the density due to less densification with increasing the free volume of the material and decreased its density [38] as a result of the presence of some glassy matrix in-between crystals of the formed microstructure as seen in Fig. 3(b). Generally, the degree of crystallinity of the glass-ceramic is more effective in their corresponding densities [39]. So, the density values of the WD3, and WD4 glass-ceramic samples were more than that of WD1, P_2O_5- free

sample, which improved the crystallization process and increase the crystallinity of the investigated glass-ceramics and led to form denser microstructure, as shown in SEM micrographs (Fig. 3c and d).

3.5. The mechanical properties (Microhardness)

Bones in the body are constantly subject to changing mechanical stresses due to the variety of body movements. So the mechanical feature is very important and must be taken into account when designing glass-ceramic materials for use in bone tissue in bioengineering applications [11]. The mechanical properties of glass-ceramics mainly depend on the mechanical characteristics of the crystalline phases formed, including the internal microstructure of their crystals, the interfacial bonding among the crystals, and vitreous phases formed in-between, as well as, the ability of the crystals to condense. The microhardness property for the resulting glass-ceramics was determined by Vicker's microhardness to reach the suitable data which are comparable with those of human bone (680–8000 MPa) [40]. The average hardness data measured for the prepared glass–ceramic species are displayed in Table 2 and Fig. 4b. The results showed that the synthesized glass-ceramics were presented good mechanical properties with high microhardness values of around 4560–5015 MPa. This may be attributed to the presence of high mechanical properties of pyroxene members [34], diopside, and wollastonite, as the major crystalline phases. The replacement of sodium calcium phosphate at the expense of diopside components explaining the decrease in the microhardness value observed for the resultant WD2 sample (4560 MPa) compared to the WD1 sample (4850 MPa) due to the formation of considerable volume fractions of a mechanically weaker $NaCa(PO_3)_3$ phase instead of a mechanically stronger diopside phase [12]. While the hardness values were increased significantly for WD3 and WD4 samples, reaching 5045 MPa and 5015 MPa, respectively. Kansal, et al. [13] reported that the combination of high mechanically bioactive material of pyroxene members as diopside $CaMgSi_2O_6$ and wollastonite-$CaSiO_3$ phases with resorbable composite such as fluorapatite-$Ca_5(PO_4)_3F$ led to the development of glass-ceramic materials with good mechanical strength and distinct biologically active properties.

Table 2
Heat-treatment regime according to Tg and Tc of the DTA analysis, crystalline phases formed, density (g/cm^3), Vicker`s microhardness (MPa), theoretical atomic Ca/P, and atomic Ca/P resulted from EDX analysis after immersion in SBF.

Sample ID.	DTA (°C)		Heat-treatment	Crystalline phases	Density (g/cm^3)	Micro-hardness (MPa)	Starting Ca/P	Analyzed Ca/P
	Tg	Tc						
WD1	747	1038	745°C/3h 1040°C/6h	$CaMgSi_2O_6$ $CaSiO_3$	2.76	4850	N/A	3.97
WD2	733	1065	730°C/3h 1065°C/6h	$CaMgSi_2O_6$ $CaSiO_3$ $NaCa(PO_3)_3$	2.50	4560	6.70	1.91
WD3	733	1072	735°C/3h 1075°C/6h	$CaMgSi_2O_6$ $CaSiO_3$ $Ca_5(PO_4)_3F$	2.92	5045	12.94	2.46
WD4	721	1027	720°C/3h 1025°C/6h	$CaMgSi_2O_6$ $CaSiO_3$ $NaCa(PO_3)_3$ $Ca_5(PO_4)_3F$	2.90	5015	4.62	1.91

Tg; glass transation temperature, **Tc**; crystallization temperature

3.6. In vitro bioactivity test

The degradation and in vitro bioactivity tests of the glass-ceramic samples under investigation were carried out in SBF. Accordingly, the possibility of the formation of a new layer of hydroxyapatite (HAp) was examined by using SEM coupled with EDX analysis. Furthermore, the pH, weight loss %, and ion concentrations (calcium and phosphate ions) were also monitored as a function of time. Figure 5 shows SEM/EDX analysis of WD1, WD2, WD3, and WD4 glass-ceramic samples after immersion in SBF for 22 d. It can be observed from the figure that newly very small spherical aggregates were formed on the glass-ceramic surfaces, which likely assigned to precipitation of a new layer of Ca-phosphate – almost HAp – crystals. This suggestion was confirmed by EDX analysis of the glass-ceramic surfaces, where the analysis showed that the atomic percentages of Ca and P became lower than the theoretical starting percentages of those atoms. Table 2 presents the comparison between the atomic Ca/P ratio of the original composition (theoretical ratio) and the ratio calculated from EDX analysis. Where, the starting

Ca/P ratio was 6.70, 12.94, and 4.62 became 1.91, 2.46, and 1.91 for WD2, WD3, and WD4, respectively. While, there was no phosphate in the original composition of the WD1 sample, but, the measured Ca/P ratio was 3.97. These results indicated that the Ca/P ratio of the newly formed layer after immersion in SBF was close to the ratio in HAp (Ca/P = 1.67). Meanwhile, WD2 and WD4 samples were possessed the same Ca/P (1.91) and they were the closest ratios to that of HAp.

The in vitro degradation and dissolution study of bioactive glass-ceramic materials in the physiological fluids is important to give a simulated picture of the behavior of those materials inside the body. In this study, the change of pH, weight loss, and ion concentrations released in SBF was assessed. Figure 6a presents a change of pH of SBF solution as a function of time. It can be noted from the figure that the pH was abruptly increased to maximum values for all samples from 7.40 to 8.09, 7.95, 7.9, and 7.82 for WD1, WD2, WD3, and WD4, respectively, after 3 d of incubation. The pH value of the WD1 sample was significantly ($p < 0.02$) higher than other samples, whereas, WD4 was significant ($p < 0.05$) lower than the other samples at this time. After this increase was close to steady-state for WD2, WD3, and WD4 samples, while, the pH value of the solution incubated WD1 was slightly decreased to reach 7.83 at the end of incubation time, and it became significantly ($p < 0.003$) lower than the other glass-ceramic samples at this time. This difference in the pH values of incubated fluid can be explained by the weight loss and ions released from the glass-ceramic samples in the immersing solution. Figure 6b shows the cumulative wt. loss percent of WD1, WD2, WD3, and WD4 glass-ceramics as a function of time. As displayed in the figure, the weight loss % of all samples, mostly, were degraded linearly with time.

Furthermore, the WD1 sample showed the highest weight loss %, while, WD4 sample presented the lowest one. However, at the initial periods of incubation, the differences in weight loss % among all samples were insignificant ($p > 0.05$), but, they became significant at the end of incubation time ($p < 0.05$). Accordingly, the introduction of $Na_4Ca(PO_3)_6$ or $Ca_5(PO_4)_3F$ into the glass-ceramic (sample WD2 and WD3, respectively) was decreased the degradation, and consequently, the reaction with SBF of the resulted glass-ceramics, and this effect become obvious when both phases were introduced in the glass composition. It has been reported that the fluoride ions decrease the glass reactivity in the solution. Accordingly, the addition of fluoride, as a fluorapatite apatite phase, into the glass composition was acted as a corrosion inhibitor [41]. And so, the existence of fluorapatite crystals in the glass-ceramic was decreased its degradation in SBF.

Figure 6. weight loss % ($.g^{-1}.d^{-1}$), pH, Ca and P ions concentrations (mM), a, b, c and d, respectively, for WD1, WD2, WD3 and WD4 samples immersed in SBF up to 22 d.

Table 3
The weight loss % rate ($g^{-1}.d^{-1}$), release rates ($mM•d^{-0.5}$) of Ca^{2+} and PO_4^{3-} from the glass-ceramic samples immersed in SBF. R^2 is the coefficient of determination.

	Wt. loss ($\%.g^{-1}.d^{-1}$)	R^2	Ca^{2+} ($mM.d^{-0.5}$)	R^2	PO_4^{3-} ($mM.d^{-0.5}$)	R^2
WD1	1.00	0.9669	2.00	0.9648	1.93	0.9978
WD2	0.58	0.9907	2.08	0.9911	1.86	0.997
WD3	0.74	0.99	1.79	0.9921	1.87	0.9952
WD4	0.42	0.9926	2.13	0.994	1.98	0.9949

3.7. Cell viability test

The in vitro cytotoxicity of WD1,WD2,WD3 and WD4 samples was evaluated against normal fibroblast Vero cells using the MTT assay [42]. Figure 7a shows the cell viability % of WD1, WD2, WD3, and WD4 samples at different concentrations (500, 250, 125, 62.5, 31.25 and 15.63 $mg.ml^{-1}$). From the figure it was generally noticed that the cell viability was decreased at high concertations, 500 and 250 $mg.ml^{-1}$ for all samples, while, the viability of cells was increased with a decrease of concentrations (from 125 $mg.ml^{-1}$ to 15.63 $mg.ml^{-1}$). On the other hand, the glass-ceramic combined fluorapatite phase (sample WD3) was showed higher cell viability than other samples at 62.5 $mg.ml^{-1}$, whereas, the glass-ceramic contained sodium calcium phosphate phase (WD2) demonstrated higher cell viability than the other glass-ceramics at high concentrations (> 62.5 $mg.ml^{-1}$). The CC_{50} values are shown in Fig. 7b as common parameters for the cytotoxicity of the investigated compounds. It is the cytotoxic concentration of the material to cause death to 50% of viable cells. The calculated CC_{50} values were about 141, 162, 121, and 116 $mg.ml^{-1}$ for WD1, WD2, WD3, and WD4, respectively. Where, WD2 (162 $mg.ml^{-1}$) sample was demonstrated the highest CC50 value, while, WD4 was showed the lowest one (116 $mg.ml^{-1}$). And so, combining of sodium calcium phosphate ($Na_4Ca(PO_3)_6$) in wollastonite-diopside glass-ceramic was presented less cytotoxic effect than that included fluorapatite ($Ca_5(PO_4)_3F$), and a combining of both crystalline phases has increased the cytotoxicity to the highest value. This can be explained by the degradation behavior of the samples in the aqueous solution. According to the degradation results, WD4 was showed a lower degradation rate and higher released Ca^{2+} ion concentration than WD2 and WD3 samples. This released high Ca^{2+} ion was increased the calcium ion concentration in the cell culture medium which may result in cell death, as reported previously [43, 44].

The photos seen under an inverted microscope for the Vero cells after incubation with all samples for 24 h confirmed the results of MTT assay in which different morphological changes and loss of adhesion to a substratum were observed at a higher concentration for WD1, WD2, WD3, and WD4. Unlike, the control cells showed adherent growth and a regular polygonal shape, While at lower concentration the adherent

ability increased with normal cell morphology and few round cells representing cellular outgrowth. Studies were found that suitable divalent ions such as $Ca^{2+}$and Mg^{2+} ions can promote cell attachment, growth, and differentiation due to cell adhesion molecules on cell surfaces [45–48].

4. Conclusion

In the current work, considerable combinations between bioactive multiphase glass-ceramic had been proposed depending on wollastonite-diopside/ sodium calcium phosphate and/or fluorapatite aiming to synthesize bioactive glass-ceramic materials with talent mechanical, chemical, and biological properties required for biomedical application. The crystallization characteristics and resultant microstructure were described by DTA, XRD, and SEM. The biological activity was studied through in vitro test by simulated body fluid (SBF), whereas, the cell viability test was estimated with the Vero cells. As well as the density and microhardness of the prepared materials were also evaluated. A bioactive phases including $CaMgSi_2O_6$, $CaSiO_3$, $NaCa(PO_3)_3$, and $Ca_5(PO_4)_3F$ were identified by XRD study after controlled heat-treatment. The studied glass-ceramics had microhardness values (4560–5045 MPa), in the ranged with those of natural human bone, and density values ranged between (2.50–2.92 $g.cm^{-3}$). The cell viability test showed that a combining of sodium calcium phosphate ($Na_4Ca(PO_3)_6$) in wollastonite-diopside glass-ceramic was obviously presented less cytotoxic effect than that included fluorapatite ($Ca_5(PO_4)_3F$), and a combining of both crystalline phases was increased the cytotoxicity to the highest value. It could be concluded therefore that the produced glass-ceramics are promising candidate materials for biomedical application and can be used for natural bone replacements in human medicine.

Declarations

Conflicts of interest

The authors declare that they have no conflict of interest.

Acknowledgement

The authors would like to thank the National Research Center, Faculty of Science, and Al-Azhar University (Girls), Egypt for the possibility to use their facilities.

References

1. Hench LL et al (1971) Bonding mechanisms at the interface of ceramic prosthetic materials. J Biomed Mater Res 5(6):117–141
2. Salinas A et al (2000) In vitro bioactivity of glass and glass-ceramics of the 3CaO· P2O5–CaO· SiO2–CaO· MgO· 2SiO2 system. Biomaterials 21(3):251–257

3. Hench LL, *An introduction to bioceramics*. Vol. 1 (1993) World scientific
4. Hench LL (1991) Bioceramics: from concept to clinic. Journal of the american ceramic society 74(7):1487–1510
5. Baino F et al (2016) Design, selection and characterization of novel glasses and glass-ceramics for use in prosthetic applications. Ceram Int 42(1):1482–1491
6. Hoppe A, Güldal NS, Boccaccini AR (2011) A review of the biological response to ionic dissolution products from bioactive glasses and glass-ceramics. Biomaterials 32(11):2757–2774
7. Montazerian M, Dutra E, Zanotto (2016) History and trends of bioactive glass-ceramics. Journal of Biomedical Materials Research Part A 104(5):1231–1249
8. Reddy AA et al (2012) Diopside–Mg orthosilicate and diopside–Ba disilicate glass–ceramics for sealing applications in SOFC: sintering and chemical interactions studies. international journal of hydrogen energy 37(17):12528–12539
9. Donald I (2007) Immobilisation of radioactive and non-radioactive wastes in glass-based systems: an overview. Glass technology 48(4):155–163
10. De Aza PN, Luklinska ZB, Anseau M, *Bioactivity of diopside ceramic in human parotid saliva*. Journal of Biomedical Materials Research Part B: Applied Biomaterials: An Official Journal of The Society for Biomaterials, The Japanese Society for Biomaterials, and The Australian Society for Biomaterials and the Korean Society for Biomaterials, 2005. 73(1): p. 54–60
11. Kapoor S et al (2016) Alkali-free bioactive diopside–tricalcium phosphate glass-ceramics for scaffold fabrication: Sintering and crystallization behaviours. J Non-Cryst Solids 432:81–89
12. Kapoor S et al (2013) Thermo-mechanical behaviour of alkali free bioactive glass-ceramics co-doped with strontium and zinc. J Non-cryst Solids 375:74–82
13. Kansal I et al (2010) Structural analysis and thermal behavior of diopside–fluorapatite–wollastonite-based glasses and glass–ceramics. Acta Biomater 6(11):4380–4388
14. Kansal I et al (2011) Diopside (CaO· MgO· 2SiO 2)–fluorapatite (9CaO· 3P 2 O 5· CaF 2) glass-ceramics: potential materials for bone tissue engineering. J Mater Chem 21(40):16247–16256
15. Abo-Mosallam H et al (2010) MAS-NMR studies of glasses and glass-ceramics based on a clinopyroxene–fluorapatite system. J Mater Chem 20(4):790–797
16. Nakajima S et al (1989) Physicochemical characteristics of new reinforcement ceramic implant. Shika gakuho Dental science reports 89(11):1709–1717
17. Kokubo T et al (1986) Formation of a high-strength bioactive glass-ceramic in the system MgO-CaO-SiO 2-P 2 O 5. Journal of Materials Science 21(2):536–540
18. Soares VO et al (2018) New sintered wollastonite glass-ceramic for biomedical applications. Ceram Int 44(16):20019–20027
19. Kokubo T (1991) Bioactive glass ceramics: properties and applications. Biomaterials 12(2):155–163
20. Elsayed H et al (2019) Comparative Analysis of Wollastonite-Diopside Glass-Ceramic Structures Fabricated via Stereo-Lithography. Adv Eng Mater 21(6):1801160

21. Fiocco L et al (2015) Bioactive wollastonite-diopside foams from preceramic polymers and reactive oxide fillers. Materials 8(5):2480–2494
22. He D et al (2016) 3D printing of Mg-substituted wollastonite reinforcing diopside porous bioceramics with enhanced mechanical and biological performances. Bioactive materials 1(1):85–92
23. Shen J et al (2020) Direct ink writing core-shell Wollastonite@ Diopside scaffolds with tailorable shell micropores favorable for optimizing physicochemical and biodegradation properties. J Eur Ceram Soc 40(2):503–512
24. Kaur P et al (2017) *Investigation of bioactive CaO-P2O5-MgO-SiO2 ceramic composition for orthopedic applications*. in *AIP Conference Proceedings*. AIP Publishing LLC
25. Hill R et al (2004) The influence of strontium substitution in fluorapatite glasses and glass-ceramics. J Non-Cryst Solids 336(3):223–229
26. Kokubo T et al (1982) *Apatite-and wollastonite-containg glass-ceramics for prosthetic application.* Bulletin of the Institute for Chemical Research. Kyoto University 60(3–4):260–268
27. Tulyaganov D. *Phase separation and devitrification in the fluorapatite–diopside system*. in *XIX Proceeding of the International Congress on Glass*. 2001
28. Kansal I, *Diopside-Fluorapatite-Wollastonite Based Bioactive Glasses and Glass-ceramics*. 2015, Universidade de Aveiro (Portugal): Ann Arbor. p. 173
29. Tulyaganov D et al (2011) Synthesis, bioactivity and preliminary biocompatibility studies of glasses in the system CaO–MgO–SiO 2–Na 2 O–P 2 O 5–CaF 2. Journal of Materials Science: Materials in Medicine 22(2):217–227
30. Salman S et al (2009) In vitro bioactivity of glass–ceramics of the CaMgSi2O6–CaSiO3–Ca5 (PO4) 3F–Na2SiO3 system with TiO2 or ZnO additives. Ceramics international 35(3):1083–1093
31. Kokubo T, Takadama H (2006) How useful is SBF in predicting in vivo bone bioactivity? Biomaterials 27(15):2907–2915
32. Cheng Y-L et al (2003) Acetone extract of Bupleurum scorzonerifolium inhibits proliferation of A549 human lung cancer cells via inducing apoptosis and suppressing telomerase activity. Life sciences 73(18):2383–2394
33. Roberts J, Mcmillin P (1979) Glass-Ceramics, Non-Metallic Solids. Academic Press Inc., London
34. Deer W, Howie R, Zussman A (1992) An Introduction to the Rock Forming Minerals, Third ELBS Impression. Printing Press Ltd., Hong Kong, Common Wealth
35. Kaur G et al (2019) Mechanical properties of bioactive glasses, ceramics, glass-ceramics and composites: State-of-the-art review and future challenges. Materials Science Engineering: C 104:109895
36. Taniguchi T, Okuno M, Matsumoto T (1997) X-ray diffraction and EXAFS studies of silicate glasses containing Mg, Ca and Ba atoms. J Non-Cryst Solids 211(1–2):56–63
37. Liu Y et al., *Nucleation and growth of needle-like fluorapatite crystals in bioactive glass–ceramics*. Journal of non-crystalline solids, 2008. 354(10–11): p. 938–944

38. Boccaccini A et al (1996) Densification and crystallization of glass powder compacts during constant heating rate sintering. Materials Science Engineering: A 219(1–2):26–31
39. Xia L et al (2011) Mechanical and thermal expansion properties of β-eucryptite prepared by sol–gel methods and hot pressing. Materials Design 32(5):2526–2531
40. Holand W, Beall GH, *Glass-ceramic technology* (2019) John Wiley & Sons
41. Brauer DS et al (2010) Fluoride-containing bioactive glasses: effect of glass design and structure on degradation, pH and apatite formation in simulated body fluid. Acta Biomater 6(8):3275–3282
42. Vega-Avila E, Pugsley MK. *An overview of colorimetric assay methods used to assess survival or proliferation of mammalian cells*. in *Proc West Pharmacol Soc*. 2011
43. Adams CS et al (2001) Matrix regulation of skeletal cell apoptosis: role of calcium and phosphate ions. J Biol Chem 276(23):20316–20322
44. Tsang EJ et al (2011) Osteoblast interactions within a biomimetic apatite microenvironment. Ann Biomed Eng 39(4):1186–1200
45. Numata T, Okada Y (2008) Molecular determinants of sensitivity and conductivity of human TRPM7 to Mg2 + and Ca2+. Channels 2(4):283–286
46. Day ES, Osborn L, Whitty A, *Effect of divalent cations on the affinity and selectivity of α4 integrins towards the integrin ligands vascular cell adhesion molecule-1 and mucosal addressin cell adhesion molecule-1: Ca 2 + activation of integrin α4β1 confers a distinct ligand specificity.* Cell communication & adhesion (2002) **9**(4): p. 205–219
47. Abdelraof M et al (2019) Green synthesis of bacterial cellulose/bioactive glass nanocomposites: Effect of glass nanoparticles on cellulose yield, biocompatibility and antimicrobial activity. Int J Biol Macromol 138:975–985
48. Farag MM, Al-Rashidy ZM, Ahmed MM (2019) In vitro drug release behavior of Ce-doped nano-bioactive glass carriers under oxidative stress. Journal of Materials Science: Materials in Medicine 30(2):18

Figures

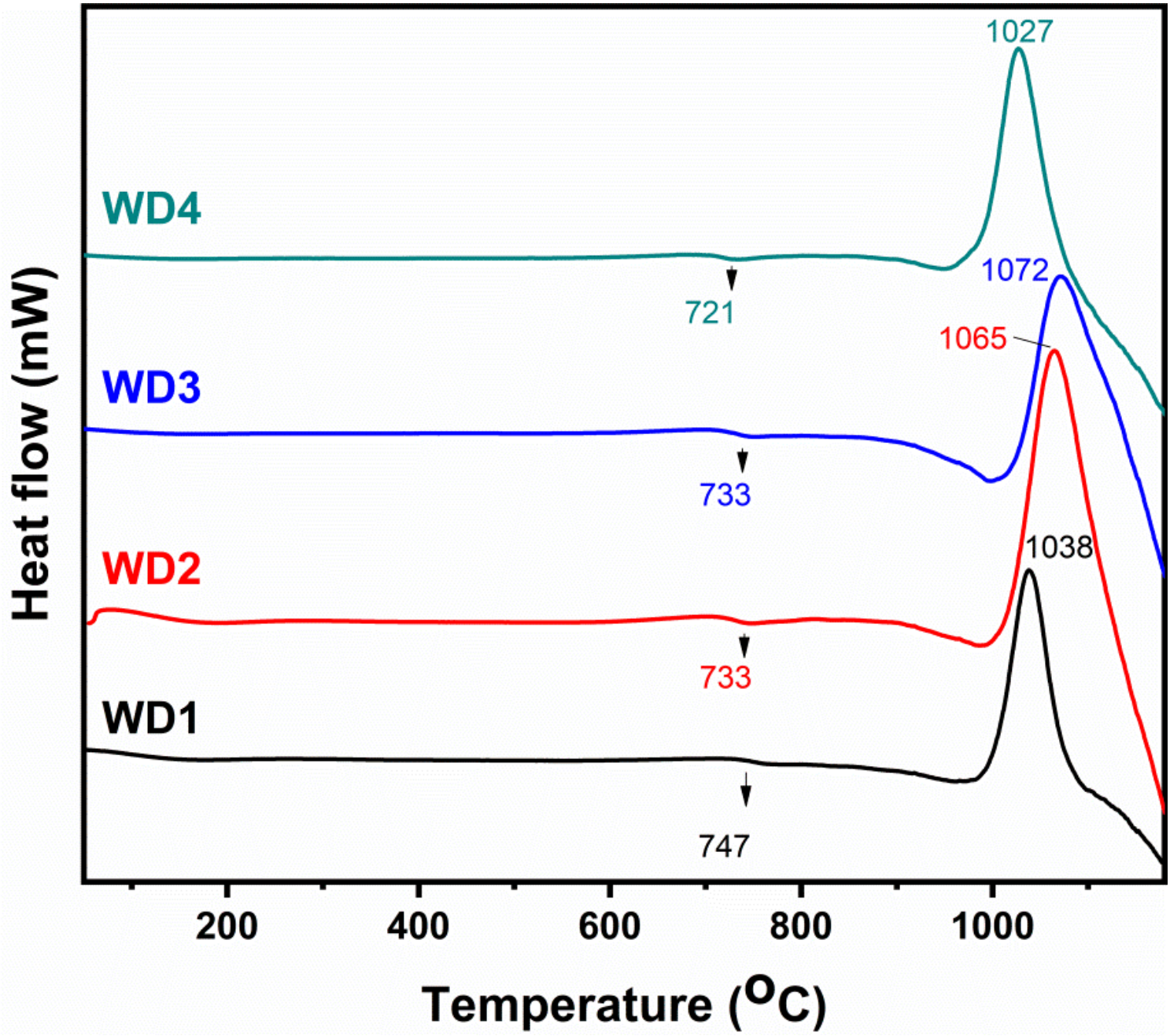

Figure 1

DTA analysis of the prepared glass samples, WD1, WD2, WD3 and WD4.

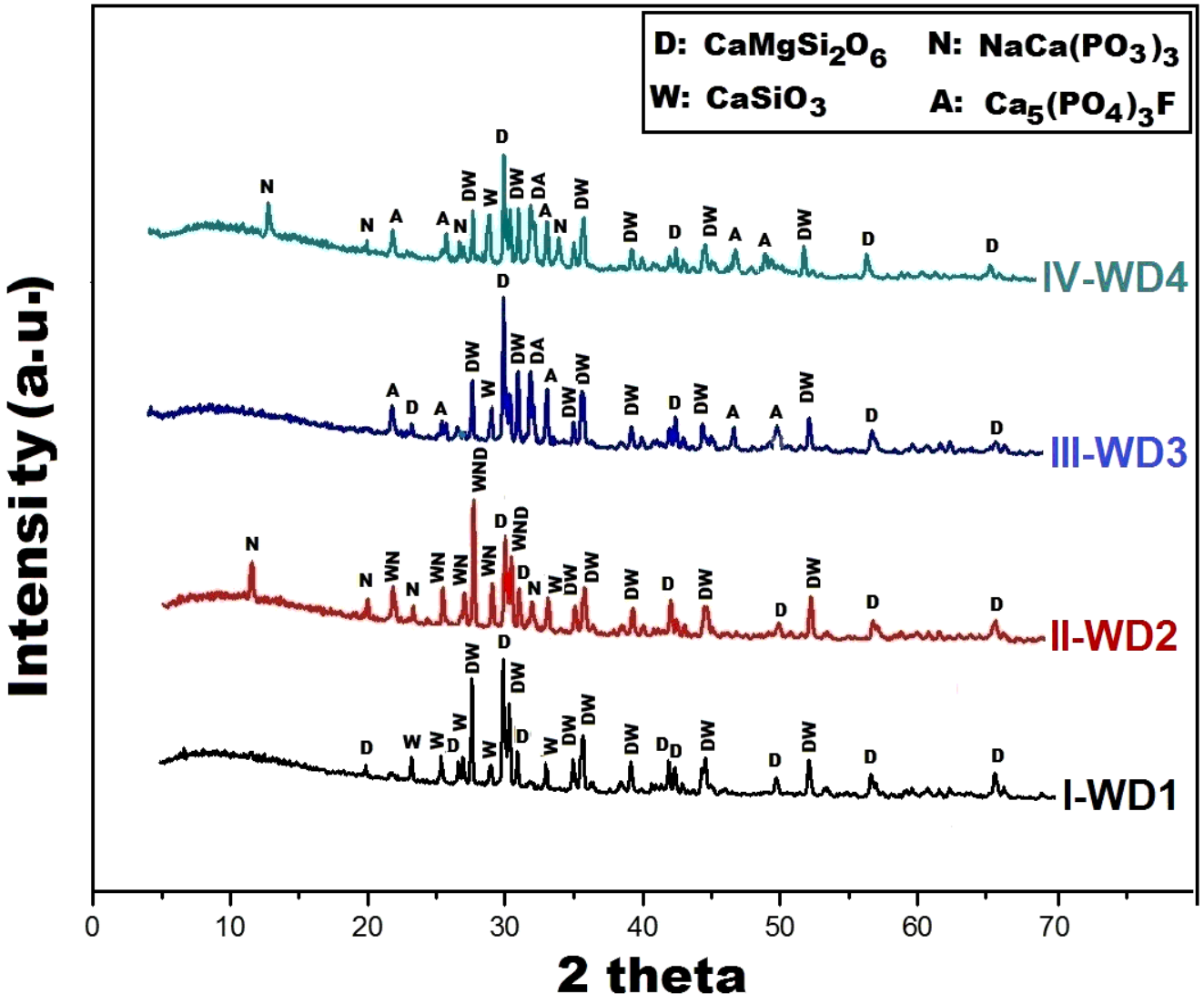

Figure 2

XRD patterns of the glass-ceramic samples WD1, WD2, WD3 and WD4.

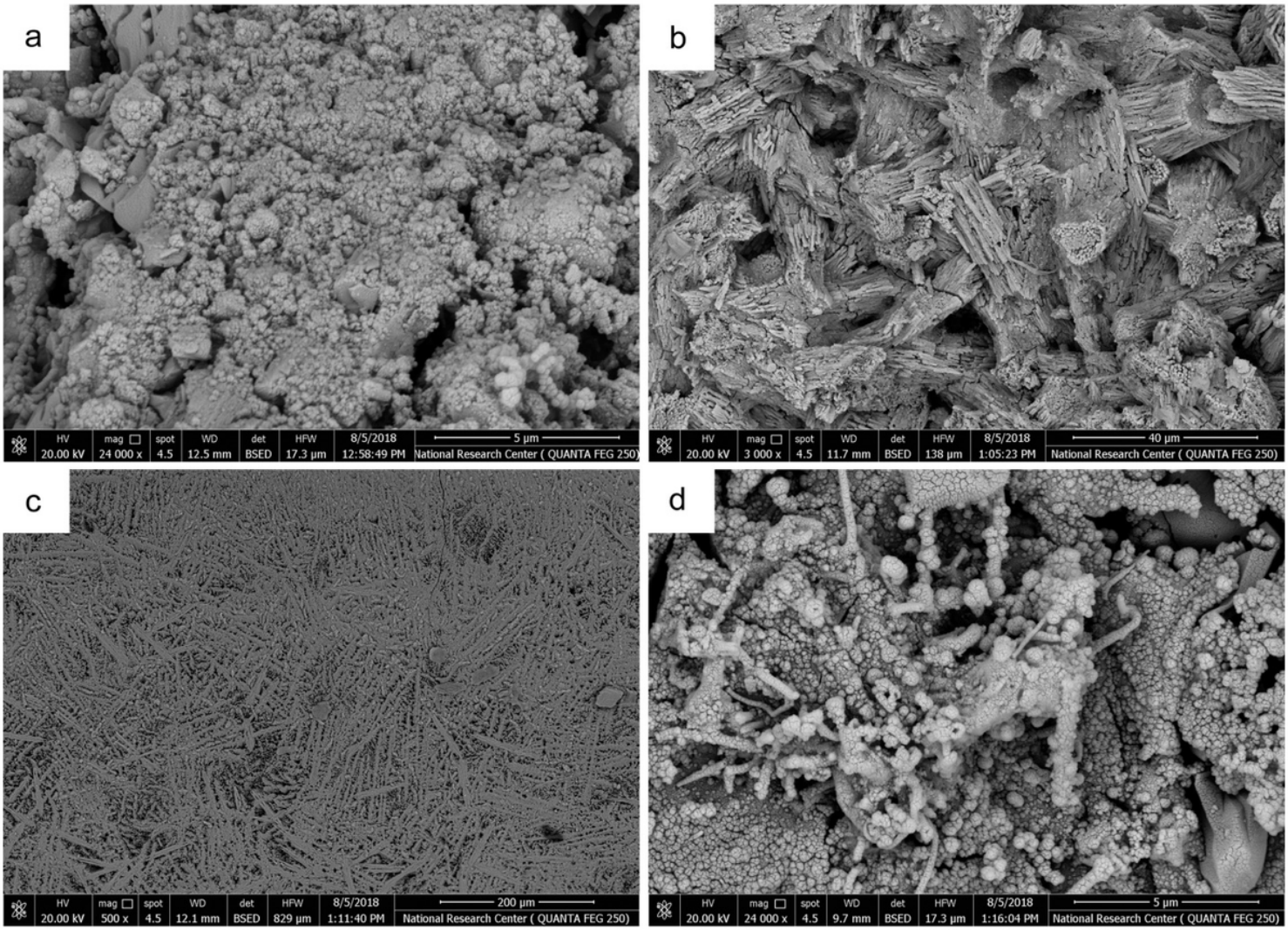

Figure 3

SEM micrographs of WD1, WD2, WD3 and WD4 glass-ceramics

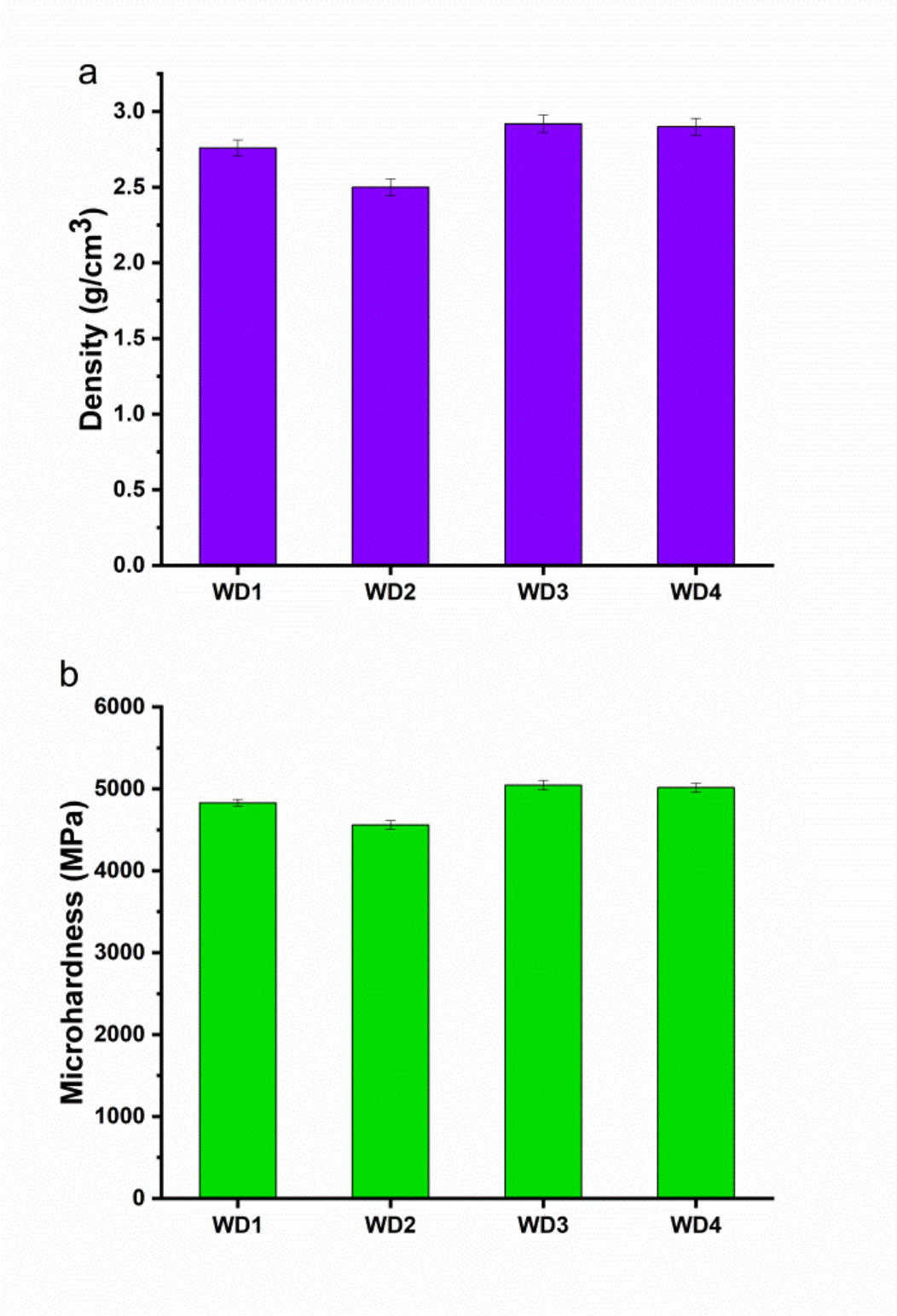

Figure 4

(a) density (cm3.g-1) and (b) Vicker`s microhardness indentation values (MPa) of WD1, WD2, WD3, and WD4 glass-ceramics.

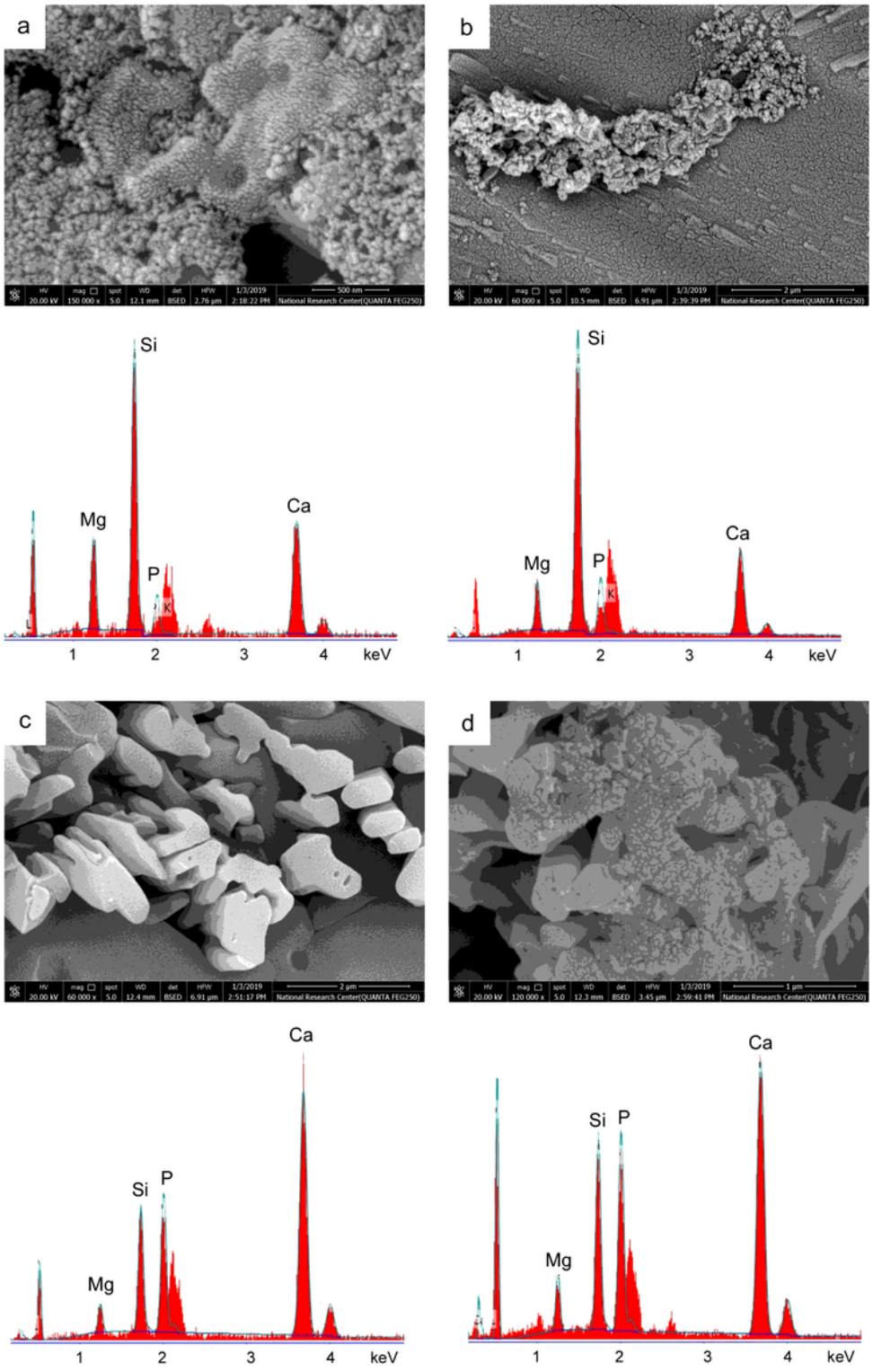

Figure 5

SEM / EDX analysis of WD1, WD2, WD3 and WD4 (a, b, c and d, respectively) after immersion in SBF for 22 d.

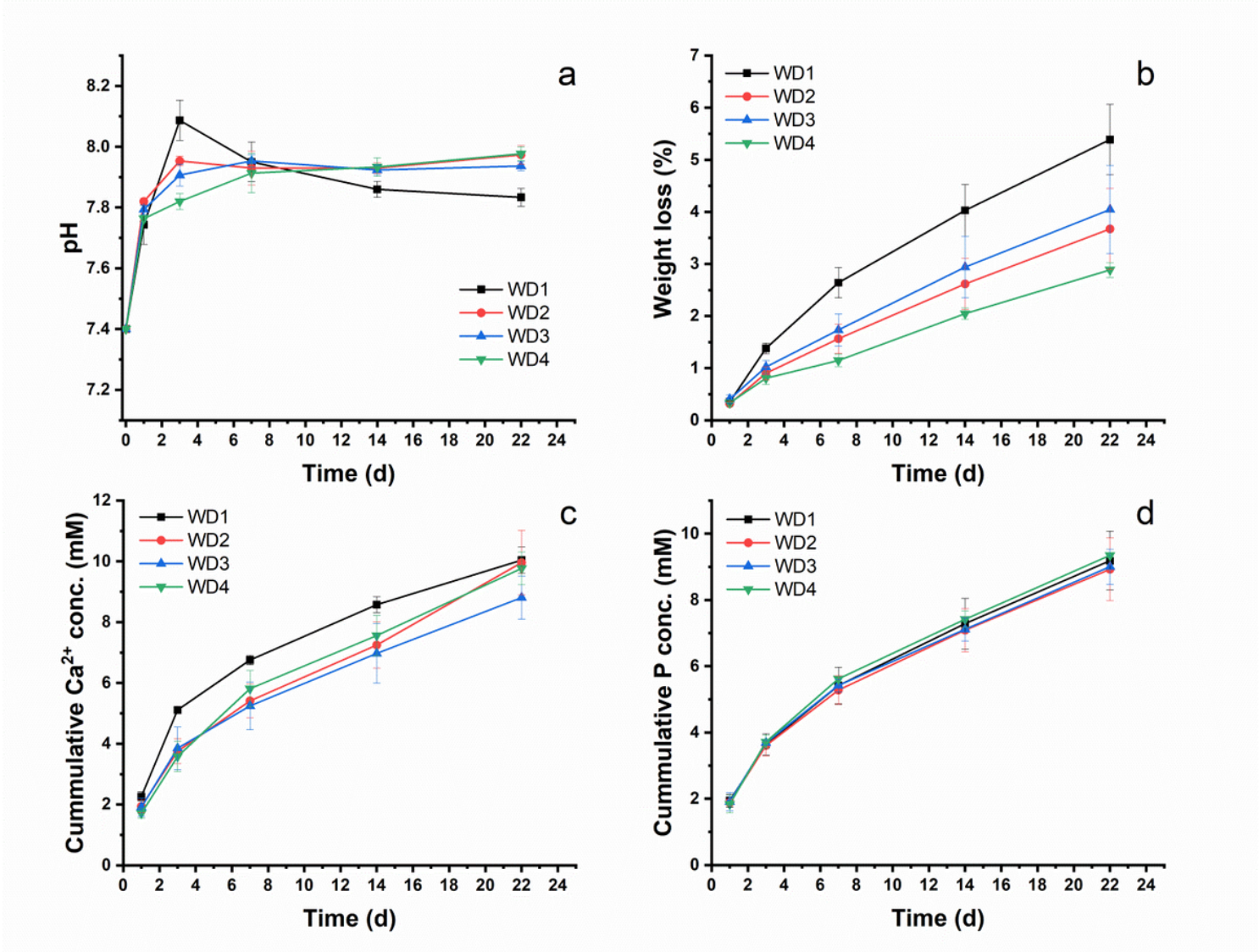

Figure 6

weight loss % (.g-1.d-1), pH, Ca and P ions concentrations (mM), a, b, c and d, respectively, for WD1, WD2, WD3 and WD4 samples immersed in SBF up to 22 d.

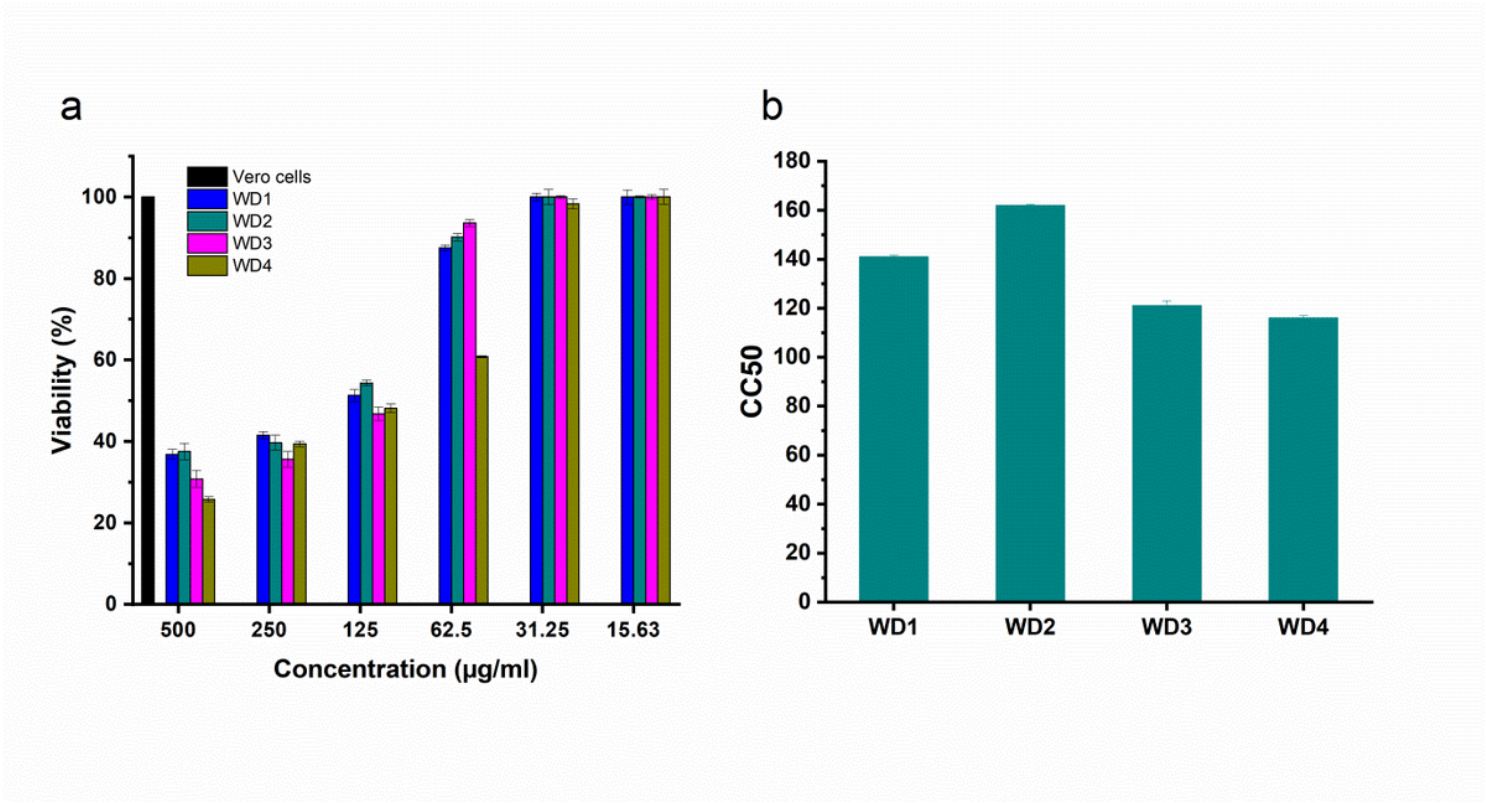

Figure 7

Cell viability % (a) and CC50 values (b) of different concentrations (500, 250, 125, 62.5, 31.25 and 15.63 mg.ml-1) of WD1, WD2, WD3, and WD4 against Vero cells, using the MTT assay.

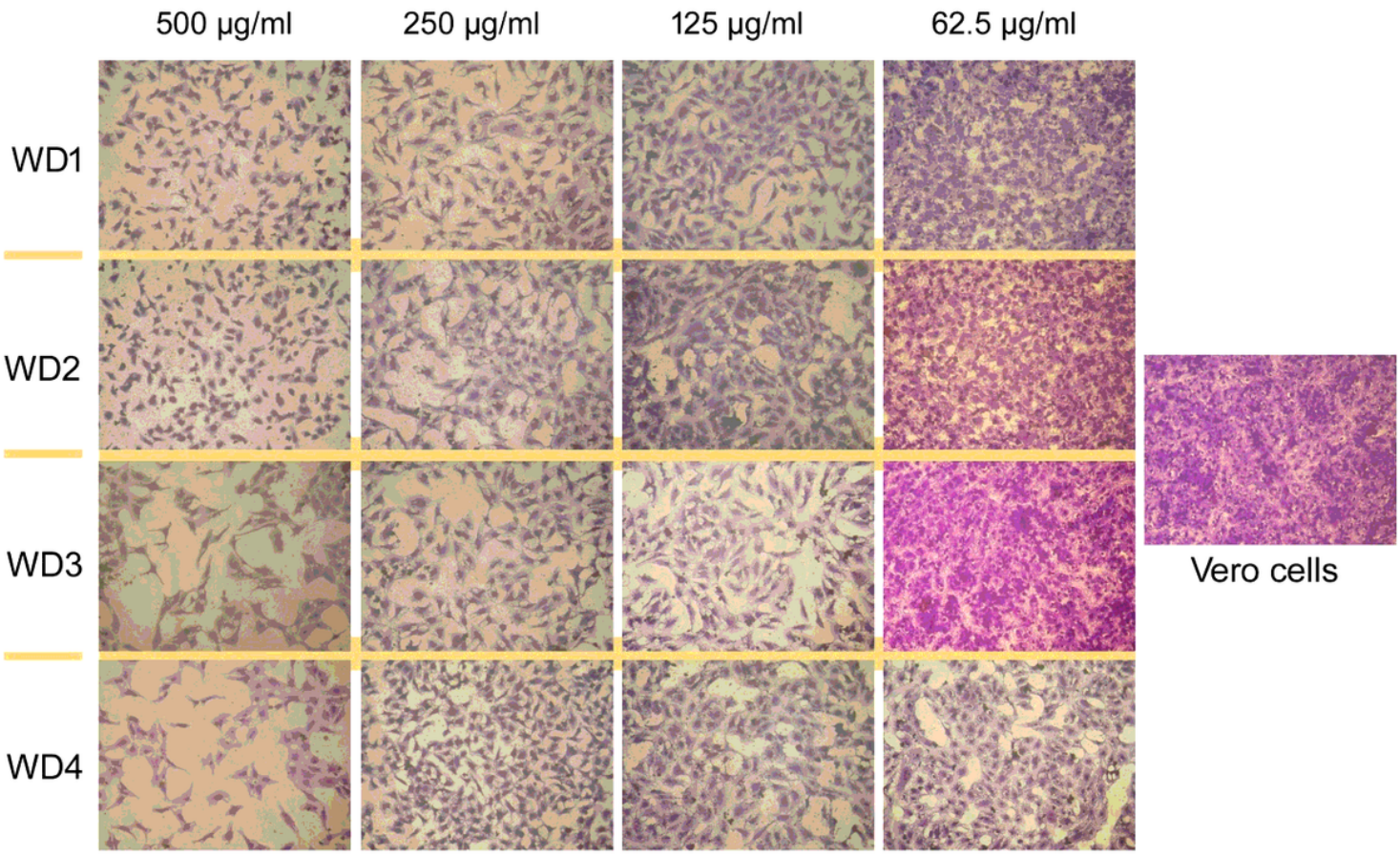

Figure 8

Inverted microscope photos of the Vero cells treated with 500 µg.ml-1 with WD1, WD2, WD3, and WD4 observed after 24 h of treatment. (Magnification: ×40)